Available online at www.sciencedirect.com
ScienceDirect
Journal of Molecular Catalysis A: Chemical 281 (2008) 49–58
JOURNAL OF MOLECULAR CATALYSIS A: CHEMICAL
www.elsevier.com/locate/molcata

Cobalt oxide surface chemistry: The interaction of CoO(1 0 0), Co_3O_4(1 1 0) and Co_3O_4(1 1 1) with oxygen and water

Sarah C. Petitto [1], Erin M. Marsh, Gregory A. Carson [2], Marjorie A. Langell *

Department of Chemistry, University of Nebraska, Lincoln, NE 68588-0304, USA

Available online 30 August 2007

Abstract

Cobalt oxides comprise two readily accessible cation oxidation states: Co^{2+} and Co^{3+}, which are thermodynamically competitive under common ambient conditions, and redox mechanisms connecting the two states are largely responsible for their success in partial oxidation catalysis. In our studies, CoO(1 0 0), Co_3O_4(1 1 0), and Co_3O_4(1 1 1) single crystal substrates have been investigated with X-ray photoelectron spectroscopy (XPS), high-resolution electron energy loss spectroscopy (HREELS), and low energy electron diffraction (LEED) for their surface reactivity toward O_2 and H_2O and for their stability under reducing UHV conditions. There is facile inter-conversion between CoO and Co_3O_4 stoichiometry at the oxide surface which, despite the compositional variability, remains well ordered in long-range structure. Surface impurities, however, can pin the surface at either CoO or Co_3O_4 compositional extremes. Contrary to reports of a pressure gap that creates difficulty in oxide hydroxylation under UHV, it is possible to hydroxylate both cobalt monoxide and spinel oxide substrates with H_2O, provided sufficient activation is available to dissociate the water molecule.

Keywords: Cobalt oxides; Rocksalt; Spinel; Epitaxial films; Water adsorption

1. Introduction

Transition metal oxides enjoy widespread use in heterogeneous catalysis [1] and gas sensing [2] due in large part to their surface redox reactivity properties. One such system comprises cobalt oxides of various composition and stoichiometry, and relies on the close thermodynamic stability of the Co^{2+}/Co^{3+} oxidation states which interconvert upon relatively mild variation in oxidizing or reducing ambient conditions. Structurally, the simplest cobalt oxide is CoO, the rocksalt monoxide, which has a single Co^{2+} octahedrally coordinated by lattice oxygen in $Fm\bar{3}m$ symmetry at 300 K [3]. Below its Néel temperature of 291 K [4], the crystal structure is reduced to C2/m symmetry by a slight tetragonal distortion. The distortion and the antiferromagnetic character of CoO are often ignored in discussions of the surface reactivity. However, the high-spin nature of the d^7 cation results in a fairly complex electronic structure that is reflected in both valence and cobalt core level cobalt photoemission.

The spinel oxide, Co_3O_4, is readily accessible and is the thermodynamically stable form of cobalt oxide under ambient room temperature and oxygen partial pressure. The normal spinel structure is $Fd\bar{3}m$, with octahedrally coordinated Co^{3+} and tetrahedrally coordinated Co^{2+} [5]. The spinel also undergoes transition to an antiferromagnetic phase, however the low spin d^6 Co^{3+} is diamagnetic and the weak magnetic coupling among the tetrahedral Co^{2+} results in a much lower Néel temperature of approximately 40 K [6]. While the electronic structure has not been studied in as much detail as has that of the monoxide, the photoemission is considerably less complex in peak shape, again due to the filled t_{2g} octahedral Co^{3+} and the weaker interaction among the tetrahedral Co^{2+}.

Upon first impressions, the spinel might appear to be considerably more structurally complex than the simple rocksalt CoO. Although both are cubic, the Co_3O_4 unit cell length at 8.084 Å is considerably larger than the 4.267 Å of the rocksalt and the cell comprises 56 ions compared to the rocksalt's four. However, the two structures are easily related through their oxygen sublattice. Both spinel and rocksalt lattice oxygen are face centered cubic (fcc), with the O^{2-}–O^{2-} closest packing distance in the rocksalt ~5% larger than in the spinel. The greater complexity for

* Corresponding author at: 629 Hamilton Hall, University of Nebraska, Lincoln, NE 68588-0304, USA. Tel.: +1 402 472 2702; fax: +1 402 472 9402.
E-mail address: mlangell@unlserve.unl.edu (M.A. Langell).
[1] Present address: Department of Chemistry and Biochemistry, University of Alaska Fairbanks, Fairbanks, AK 99775, USA.
[2] Present address: Department of Chemistry and Physics, Mansfield University, Grant Science Building, Mansfield, PA 16933, USA.

1381-1169/$ – see front matter © 2007 Elsevier B.V. All rights reserved.
doi:10.1016/j.molcata.2007.08.023

the spinel results from the cation distribution, which produces a decrease in the overall crystal symmetry and a larger unit cell. All octahedral sites are filled in the rocksalt but only half are filled in the spinel, and the tetrahedral sites, which are completely unoccupied in rocksalt, are partially filled to one-eighth occupancy in the spinel.

In our studies, CoO(1 0 0), Co_3O_4(1 1 0) and Co_3O_4(1 1 1) single crystal substrates have been investigated with X-ray photoelectron spectroscopy (XPS), high-resolution electron energy loss spectroscopy (HREELS), and low energy electron diffraction (LEED) for their surface reactivity toward O_2 and H_2O and for their stability under reducing UHV conditions. Co^{2+}/Co^{3+} oxidation states are found to interconvert readily at the CoO(1 0 0) crystal surface upon mild changes in oxidizing and reducing conditions, and Co 2p XPS shows the oxidized Co^{3+} to be consistent with a low spin octahedral spinel chemical environment. The near-surface region also remains well ordered, as determined by LEED measurements, for surfaces undergoing oxidation and reduction and retains the general cubic symmetry. Some variation in oxygen environment is found in these thin films, however, which can only partially be attributed to surface hydroxylation from ambient contamination. CoO(1 0 0)/Co_3O_4 epitaxies are compared to the naturally occurring Co_3O_4(1 1 0) and Co_3O_4(1 1 1) surfaces for composition, phonon structure, and surface hydroxylation properties. Contrary to reports of a pressure gap that creates difficulty in oxide hydroxylation under UHV, it is possible to hydroxylate the oxide substrates with H_2O, provided sufficient activation is available to dissociate the water molecule.

2. Experimental

CoO single crystal samples, grown by flame fusion, were obtained from Atomergic Chemetals and were oriented by back Laue X-ray diffraction to within 0.05° of the (1 0 0) orientation. The surface was then polished with successively finer grades of alumina to 0.03 μm particle size and ultrasonicated sequentially in H_2O, acetone, and methanol prior to mounting in ultrahigh vacuum (UHV) for *in situ* surface preparation. UHV conditioning was performed in repeated cycles of Ar^+ sputtering (4×10^{-3} Pa Ar, 2 kV, 3 μA/cm^2, 15 min), oxygen annealing (7×10^{-5} Pa O_2, 523 K, 15 min), and UHV annealing ($\leq 4 \times 10^{-8}$ Pa, 10 min) until the surface was stoichiometric by Auger (AES) and X-ray photoelectron (XPS) spectroscopies, and characteristic binding energies and peak shapes were achieved in XPS. This procedure is described in greater detail elsewhere [7,8]. Characteristic XPS peak shapes and surface stoichiometry were confirmed by comparison to a CoO(1 0 0) surface prepared by UHV cleavage.

Co_3O_4 single crystals were grown electrolytically from a molybdate flux [9]. The crystal morphology is that of a truncated octahedron, and well-developed Co_3O_4(1 1 0) and Co_3O_4(1 1 1) surfaces formed with dimensions of several millimeters on the side of a crystal face and were used without further orientation. Prior to mounting in UHV, the crystals were ultrasonicated as described above, and were conditioned in UHV by similar sputter/annealing cycles to the CoO(1 0 0) sample. One sample was vacuum cleaved, nominally to present the (1 1 0) surface, and the cleaved surface spectra are provided as reference.

AES and XPS data were acquired with a Physical Electronics 15-255G double pass cylindrical mirror analyzer, with the Auger data acquired in the lock-in mode at 3 eV peak to peak modulation energy, 1 eV/s scan rate, and 1 eV sampling intervals. Both 2 and 3 kV primary beam energies were employed. XPS was acquired in a constant 50 eV pass energy mode, in 0.1 eV increments at a 50 ms dwell time and was signal averaged for at least 100 scans. The system was equipped with a dual Mg Kα–Al Kα anode for photoexcitation. Peak fitting, when reported, was performed with XPSPEAK41 [10] software with a Shirley background [11,12] subtraction and 40%/60% Lorentzian/Gaussian peak shape.

High-resolution electron energy loss spectroscopy (HREELS) was performed in two different UHV systems, both equipped with four-grid retarding LEED optics and with identical AES/XPS analyzers. One HREELS spectrometer, a single-pass 127° sector analyzer, was built in-house and was used in the CoO(1 0 0) and CoO(1 0 0)/Co_3O_4 studies. The other system, used for single crystal Co_3O_4(1 1 0) and Co_3O_4(1 1 1) measurements, is a LK Technologies 2000 127° sector analyzer with a double pass monochromator. Both employed a 3.77 eV primary beam that impinged the sample at an angle 60° relative to the surface normal, with electron loss measured in the specular direction. Deconvolution [13,14] of the HREELS data was implemented in Mathematica v5.0 with the discrete Fourier transform built into the software.

3. Results

3.1. CoO(1 0 0)/Co_3O_4 epitaxy

The electronic structure of rocksalt CoO results in characteristic satellite structure in core cobalt photoemission [8,14–18], which is extremely sensitive in intensity and binding energy to the stoichiometry and order of the surface. Co 2p photoemission is shown in Fig. 1 for UHV-cleaved CoO(1 0 0) with binding energies of 780.4 eV for $2p_{3/2}$ and 796.2 eV for $2p_{1/2}$ photoemission maxima and satellite structure at 786.7 and 802.5 eV for $2p_{3/2}$ and $2p_{1/2}$, respectively, and are in agreement with literature values [18]. Binding energies were calibrated relative to the CoO O 1s peak at 529.4 eV to compensate for charging and work function effects.

Although macroscopic single crystals can be held indefinitely under laboratory conditions without significant change in the bulk composition, CoO samples are metastable under typical ambient conditions and Co_3O_4 is thermodynamically the preferred oxide form at room temperature and oxygen partial pressure [19]. Bulk thermodynamic data (Table 1) can be used to determine the threshold pressure for monoxide to spinel conversion according to Scheme 1, and these data lead to the expectation that Co_3O_4 will form spontaneously at the CoO surface under mild ambient conditions. The close relationship between the rocksalt and spinel oxygen sublattices and the ease with which cations can move between octahedral and tetrahedral

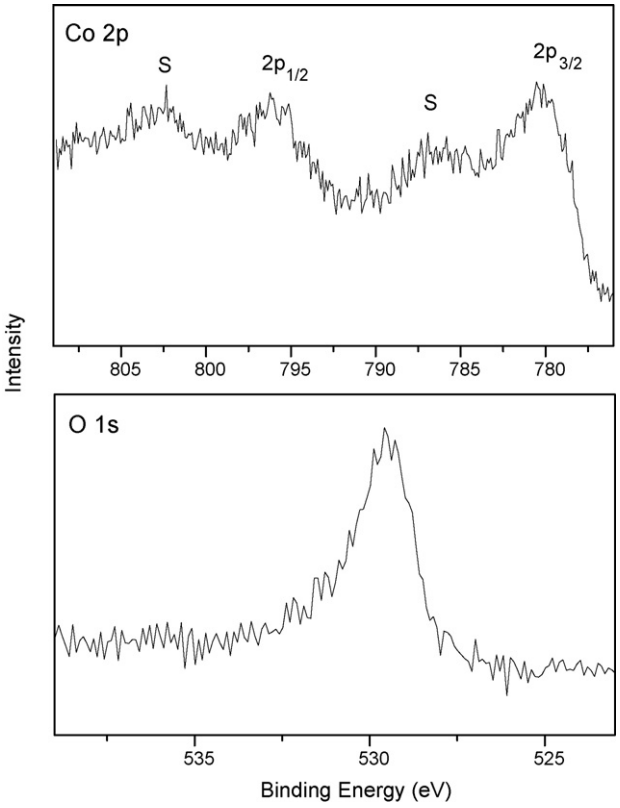

Fig. 1. Co 2p and O 1s XPS spectra for the UHV-cleaved CoO(1 0 0) acquired with Mg Kα radiation.

Table 1
Bulk thermodynamic data and threshold pressures for the CoO to Co_3O_4 conversion as a function of temperature

Temperature (K)	$\Delta G^{\circ}(T)$ (kJ)	Threshold oxygen pressure (kPa)
300	−138.29	4.34×10^{-47}
400	−124.02	3.98×10^{-31}
500	−109.20	1.50×10^{-21}
600	−94.39	3.65×10^{-15}
700	−79.58	1.33×10^{-10}
800	−64.77	3.50×10^{-7}
900	−49.96	1.60×10^{-4}
1000	−35.15	2.14×10^{-2}

Thermodynamic data are available in Ref. [19].

$$3\ CoO_{(s)} + \tfrac{1}{2}\ O_{2(g)} \rightarrow Co_3O_{4(s)}$$

$$\Delta_{rxn}G(T) = \Delta_{rxn}G^{o}(T) - RT\ \ln P^{1/2}$$

Scheme 1.

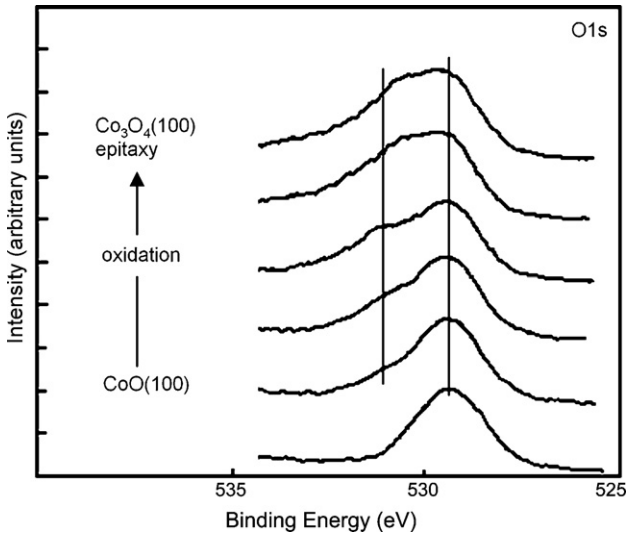

Fig. 3. O 1s XPS spectra for the O_2-annealed (1.3×10^{-2} Pa, 773 K) CoO(1 0 0) substrate. A higher binding energy peak grows in at 531.2 eV with increased O_2 exposure. The CoO oxygen lattice peak is found at 529.4 eV. XPS data were acquired with Mg Kα radiation.

sites at the surface (Fig. 2) suggest the prospect that this can be accomplished epitaxially.

CoO(1 0 0) substrates heated in UHV under O_2 show signs of surface oxidation through increased oxygen concentration and the appearance of a new feature in O 1s XPS. Fig. 3 shows the effects of oxygen annealing at 1.3×10^{-2} Pa and 773 K on the CoO(1 0 0) surface and indicates the appearance of a new peak at 531.2 eV that grows in with increased O_2 exposure and saturates after approximately 4 h at 70% of the main lattice peak intensity (Fig. 4). As the surface is oxidized, the CoO lattice O 1s peak at 529.4 eV is attenuated and the intensity decreases exponentially as expected from Frank–Van der Merwe layer by layer growth [20]. Assuming a mean free path of 11 Å and layer

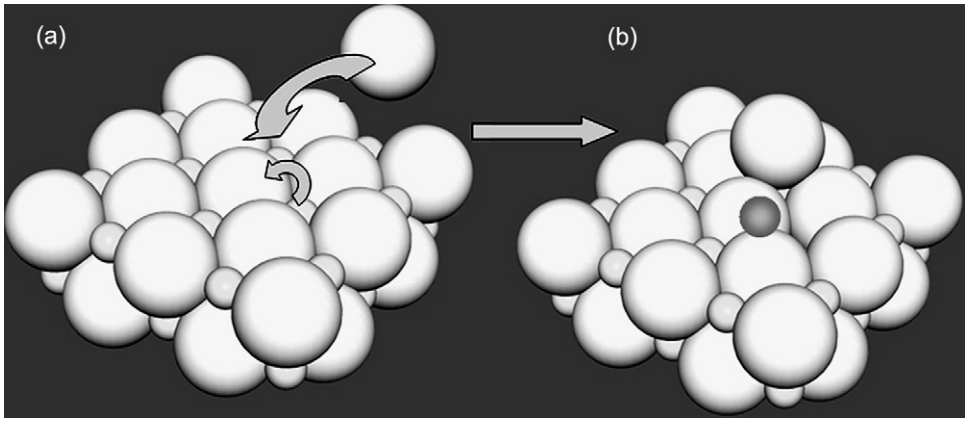

Fig. 2. Schematic diagram illustrating the ease with which a cation in an octahedral site of a rocksalt lattice can move to a tetrahedral sites at the surface.

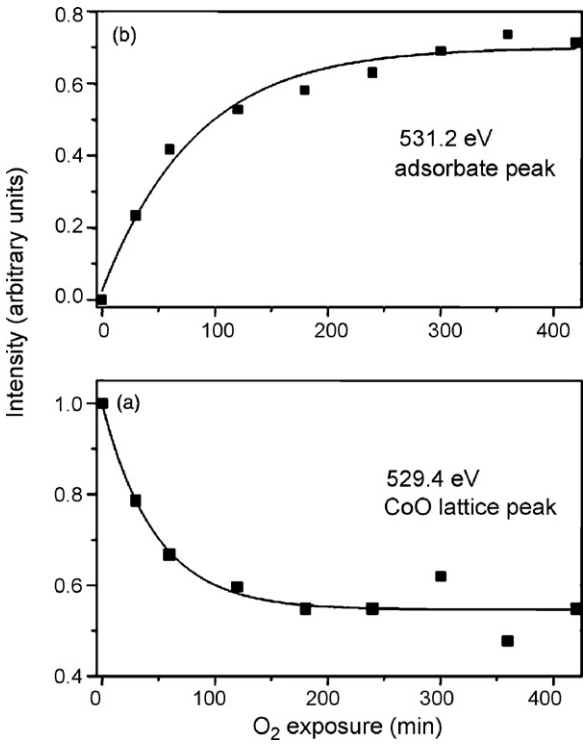

Fig. 4. O 1s XPS integrated peak intensities as a function of O_2 exposure for the CoO(1 0 0) substrate for (a) the lattice oxygen at 529.4 eV and (b) adsorbate peak at 531.2 eV.

by layer growth, the attenuation corresponds to a thickness of approximately five monolayers. Under these conditions, the saturated surface results in an epitaxial layer, as is evident in the LEED data shown in Fig. 5.

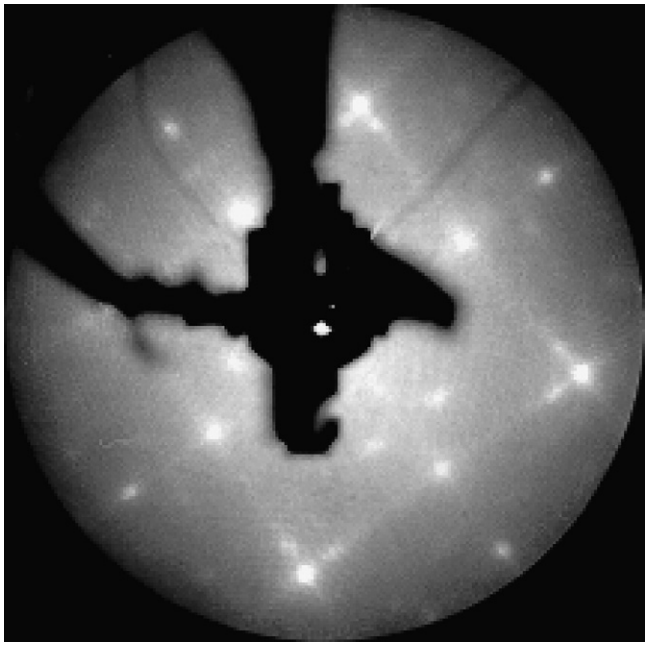

Fig. 5. LEED data for the CoO(1 0 0) surface with ~5 monolayer epitaxial layer on the resulting from the O_2 (1.3×10^{-2} Pa, 773 K) after 4 h acquired after cooling to room temperature. The pattern is acquired at an incident electron beam energy of 85 eV.

XPS of the Co 2p region is compared for CoO(1 0 0) heated under O_2 to saturation to that obtained on UHV-cleaved CoO(1 0 0) and Co_3O_4(1 1 0) crystals in Fig. 6. The oxidized CoO(1 0 0) substrate shows a characteristic sharpening of the main $2p_{3/2}$ and $2p_{1/2}$ peaks, now found at 770.8 eV and 795.7 eV, respectively, and a dramatic decrease in intensity of the satellite structure, which also shifts to higher binding energy by approximately 2 eV. The more complex structure in the CoO photoemission is a direct result of the nature of the valence band produced by octahedrally coordinated, high-spin Co^{2+} oxides. The high-spin character allows for strong electron correlation resulting in a range of closely lying states with vary d–d coupling, and the overlap of cobalt valence orbitals with surrounding O 2p allows for charge-transfer [21–23] from O 2p to the Co 3d leading to the possibility of different final states in the photoemission mechanism. These effects are not present in either low spin, octahedrally coordinated Co^{3+} or tetrahedrally coordinated Co^{2+}.

The sharper Co 2p XPS peaks and the diminished satellite intensity are compatible with Co_3O_4 thin film formation. However, the O 1s binding energy for the epitaxial layer is approximately 1 eV too high for lattice oxygen at the surface of a bulk Co_3O_4 spinel substrate, which is found at comparable values to rocksalt CoO [18]. Differential charging can be discounted as the reason for the rather substantial shift in bind-

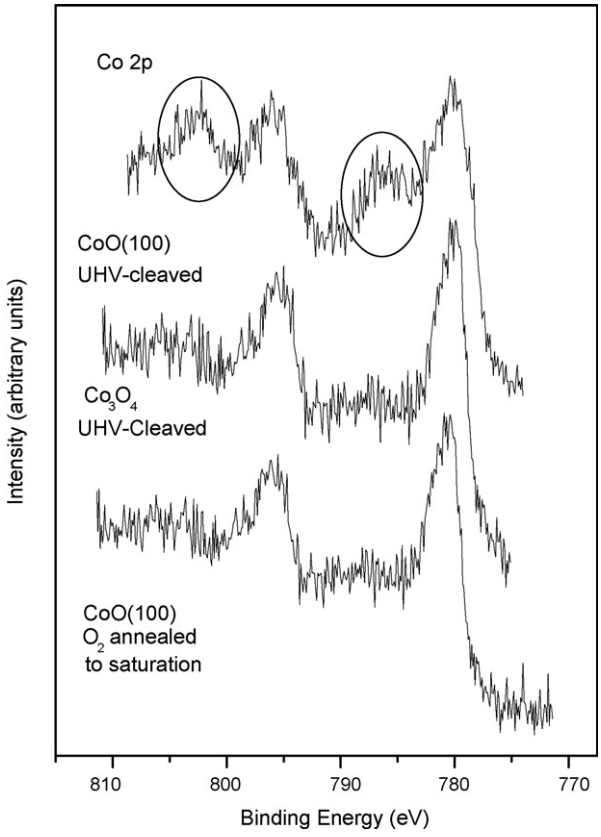

Fig. 6. Co 2p XPS region comparing the CoO(1 0 0) surface annealed to saturation under O_2 (1.3×10^{-2} Pa, 773 K) to UHV-cleaved CoO(1 0 0) and Co_3O_4(1 1 0) single crystals The satellite structure characteristic of the octahedral Co^{2+} cation is circled in the CoO(1 0 0) spectrum. The spectra were acquired with Mg Kα radiation.

ing energy, since the Co 2p peaks are found at their expected values and show no sign of charging relative to the O 1s CoO lattice peak. Surface hydroxylation can also be ruled out, since no indication of surface OH vibrations are found in the HREELS spectrum (Fig. 7). Thus, the higher binding energy of the oxygen 1s peak in the epitaxial layer must either be attributable to the defect structure of the epitaxy or inherent in the nature of the thin film.

In addition to confirming that the hydroxylation level in the thin film epitaxy is below the level of detection, and thus cannot be primarily responsible for the higher binding energy O 1s XPS peak, the HREELS data indicate the development of additional phonon structure in line with the lower symmetry of the thin film surface. In addition to adsorbate vibrational losses, ionic materials show intense electron scattering from Fuchs–Kliewer phonon modes [14,24–26]. These modes, which are the electron scattering analog of transverse optical phonons, result from a collective lattice vibration of surface ions in which the cations and anions vibrate out of phase. The large dipole resulting from the phonon motion produces a very large cross section for electron scattering and results in a series of intense substrate phonon peaks from multiple scattering events as the HREELS electron approaches and leaves the surface.

In the multiple scattering peaks, the consecutive scattering events are uncorrelated, and the intensity decreases statistically with number of scattering losses. Since all information in the multiple loss peaks is contained in the single-loss fundamental phonon spectrum, it is possible to deconvolute [13,14] the multiple scattering events from the single-loss data to free up the spectrum for vibrational analysis. Deconvolution of the CoO(1 0 0)/Co_3O_4 HREELS spectrum has been performed for the inset shown in Fig. 7. All multiple loss features have been removed, leaving the single fundamental Fuchs–Kliewer phonon mode of the rocksalt lattice at 558 cm^{-1} (69.2 meV) and two new features unique to the CoO(1 0 0)/Co_3O_4 epitaxy. The loss at 486 cm^{-1} (60.3 meV) is an additional phonon mode resulting from the lower symmetry of the epitaxial structure and the loss at 1097 cm^{-1} (136.0 meV) is assigned to a surface adsorbate, most likely residual O_2^- that forms as an intermediate in the oxidation reaction.

The additional phonon structure can be seen in the HREELS spectrum without the use of deconvolution by inspection of the gain peaks, found to the high-energy side of the elastic peak. A second phonon peak, the gain analog of the 486 cm^{-1} (60.3 meV) peak deconvoluted above, is clearly resolvable for the epitaxy produced by annealing under 1.3×10^{-2} Pa oxygen. Lower oxygen pressures result in incomplete oxidation and a smaller shift in fundamental phonon frequency for the second phonon peak.

3.2. Co_3O_4(1 1 0) surface

Due to the templating effect of the substrate, the oxidized CoO(1 0 0) surface shows square symmetry consistent with (1 0 0) orientation of the epitaxial film (Fig. 5). However, naturally occurring Co_3O_4 crystals form with (1 1 0) and (1 1 1) faces, with crystal growth morphology in the form of a truncated octahedron. The Co_3O_4(1 1 0) surface orientation of the as-grown crystal produces well-ordered substrates with rectangular surface symmetry in LEED (Fig. 8). The reduced crystal symmetry introduced by the partial octahedral and tetrahedral site occupancy can potentially result in two general types of surface termination for the (1 1 0) spinel orientation: type A which contains both octahedral and tetrahedral cobalt cations and type B in which half of the octahedral sites are occupied. Neither is completely non-polar. The LEED data have previously been shown to be consistent with type A termination for Co_3O_4(1 1 0) [8], in agreement with that observed for the related inverse spinel system of Fe_3O_4(1 1 0) [27,28]. Note that the type A surface is corrugated, with tetrahedral Co^{2+} located above the plane formed by the Co^{3+}-O^{2-} lattice net.

Co 2p XPS of the UHV-cleaved Co_3O_4(1 1 0) surface was previously shown in Fig. 6. However, it is also possible, and often more convenient to be able to prepare the sample by sputter/anneal sample conditioning, as is described in Section 2. XPS for a sputter-annealed Co_3O_4(1 1 0) surface is shown in Fig. 9, showing characteristic Co 2p peak shape and binding energies. The O 1s region is consistent with stoichiometric Co_3O_4, although the region can be fit with two peaks at 529.4 eV for the main lattice oxygen and a second much less intense

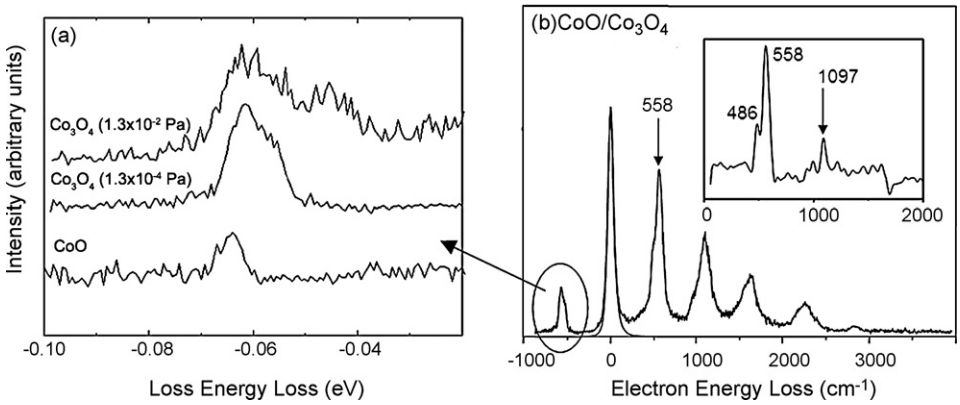

Fig. 7. HREELS of (a) cobalt oxide series showing the changes in the energy gain peak, and (b) the full spectrum of the CoO/Co_3O_4 epitaxial layer showing the electron scattering from Fuchs–Kliewer phonon modes. The inset in part (b) shows the deconvolution of the multiple scattering events to yield the single-loss data. The primary scattering beam energy is 3.77 eV.

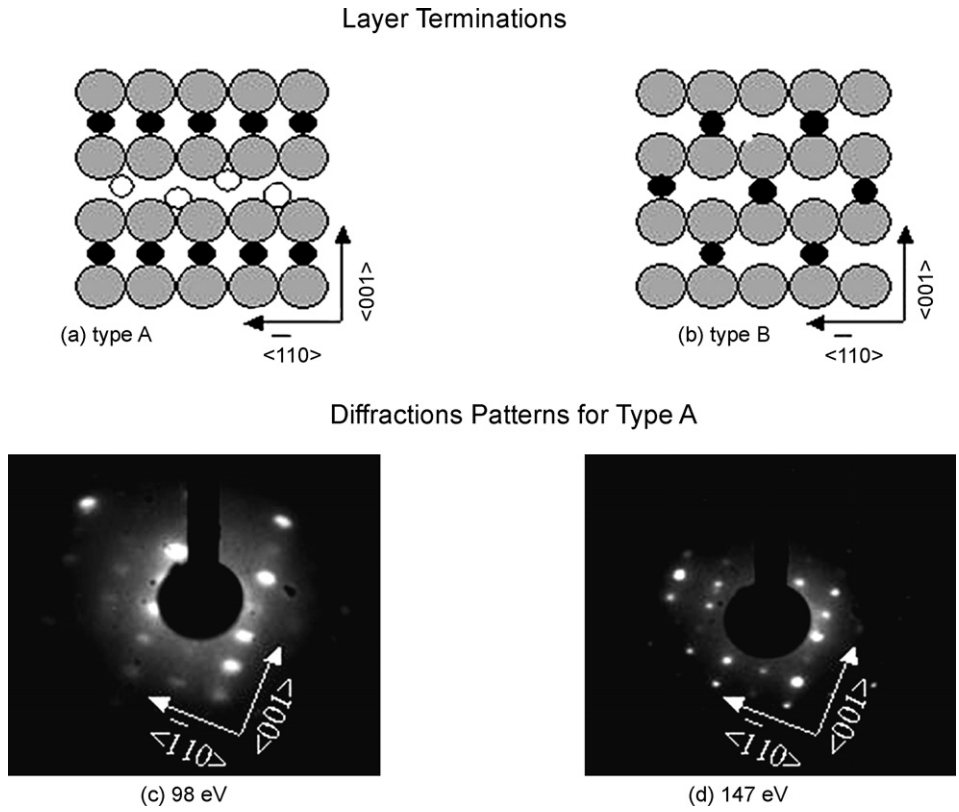

Fig. 8. A schematic of the Co_3O_4(1 1 0) two ideal bulk termination structures: (a) type A and (b) type B, and the LEED data indicating type A termination taken at (c) 98 eV and (d) 147 eV incident electron beam energies. The LEED were acquired at 300 K.

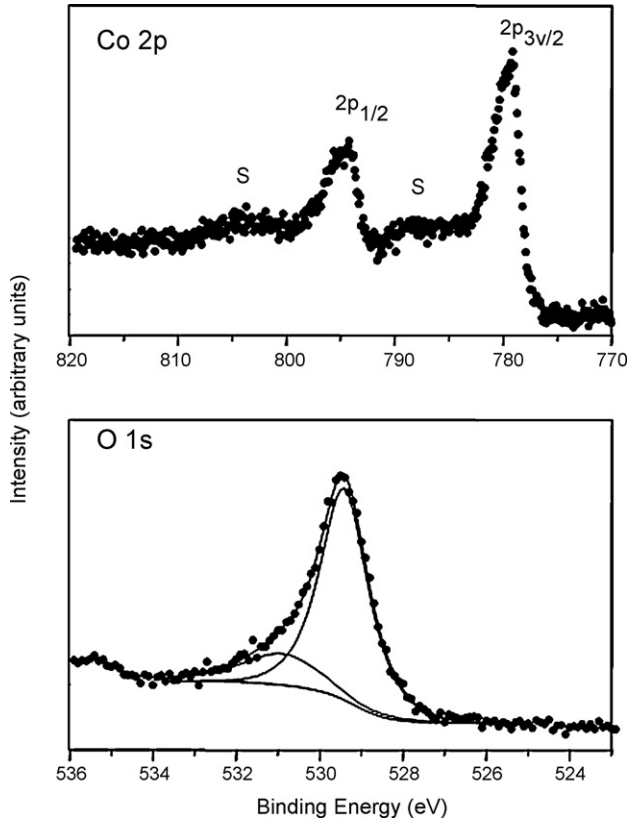

Fig. 9. XPS spectra of UHV-conditioned (sputter/anneal) Co_3O_4(1 1 0) for the Co 2p and O 1s regions. Data are acquired with Mg Kα radiation.

peak at 530.8 eV present in about 10–15% intensity of the main lattice oxygen peak. The second, less intense peak is much lower in binding energy than the CoO(1 0 0)/Co_3O_4 O 1s feature that forms upon oxidation of the CoO(1 0 0) substrate. The peak is at the level of accuracy of the background subtraction and peak fit procedure, and could result from either incomplete background removal and/or imperfect reproduction of the experimental peak shape. However, contributions to the high-binding energy peak from a surface oxygen defect species, hydroxylation from residual background water in the UHV system or oxygen adsorbate residual from the annealing procedure all remain possible.

HREELS analysis (Fig. 10) of the Co_3O_4(1 1 0) surface does reveal the presence of slight surface hydroxyl contamination, although the more striking features of the spectrum are the four well-developed phonon modes at 218, 373, 598 and 682 cm^{-1} (27.0, 46.2, 74.1, and 84.6 meV, respectively). These values are in good agreement with IR spectra [29,30] for the transverse optical phonon modes found for the spinel Co_3O_4 substrate and present a very different spectrum than that obtained on the CoO(1 0 0)/Co_3O_4 epitaxy with only two resolvable phonons at 486 and 558 cm^{-1} (60.3 and 69.2 meV). Fuchs–Kliewer phonons are collective oscillations of the lattice ions and can extend for a hundred or more angstroms into the material. The HREELS spectrum is thus still largely dominated by the CoO(1 0 0) substrate and the thin film epitaxy does not reproduce the dielectric nature sampled by the scattering HREELS electron at the Co_3O_4 bulk crystal surface.

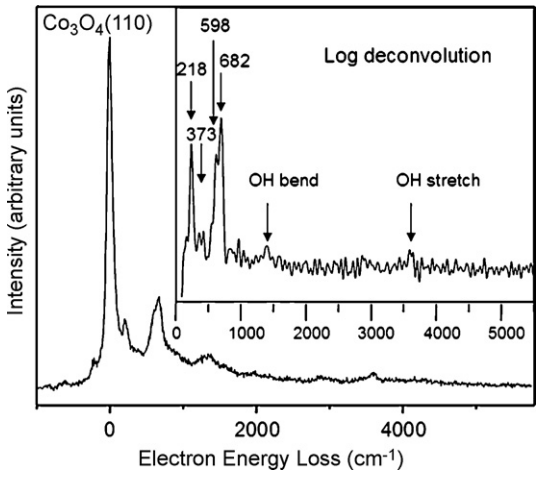

Fig. 10. HREELS spectrum of UHV-conditioned (sputter/anneal) Co_3O_4(1 1 0) with the inset showing deconvolution to reveal four well-developed phonon modes at 218, 373, 598 and 682 cm^{-1}. Data were acquired with a primary energy beam of 3.77 eV.

Heating the Co_3O_4(1 1 0) substrate under UHV causes surface reduction and the formation of a CoO-like layer, highlighting the reversible nature of the oxidation/reduction reaction of Scheme 1. In addition to an overall decrease in relative oxygen to cobalt intensity, in line with that expected for the decrease in stoichiometry, the XPS for the reduced Co_3O_4(1 1 0) indicates the formation of high spin, octahedrally coordinated Co^{2+} through the 2p satellite structure and the majority of the oxygen intensity in the single 529.4 eV lattice oxygen peak (Fig. 11). The reduction process is, in the present case, complicated by segregation of impurities from the bulk to the surface. These impurities include calcium, potassium, sodium, and copper, and the presence of copper, in particular, appears to prevent reoxidation of the substrate by the formation of a copper oxide overlayer. The segregation and reoxidation process is described in greater detail elsewhere [8,31].

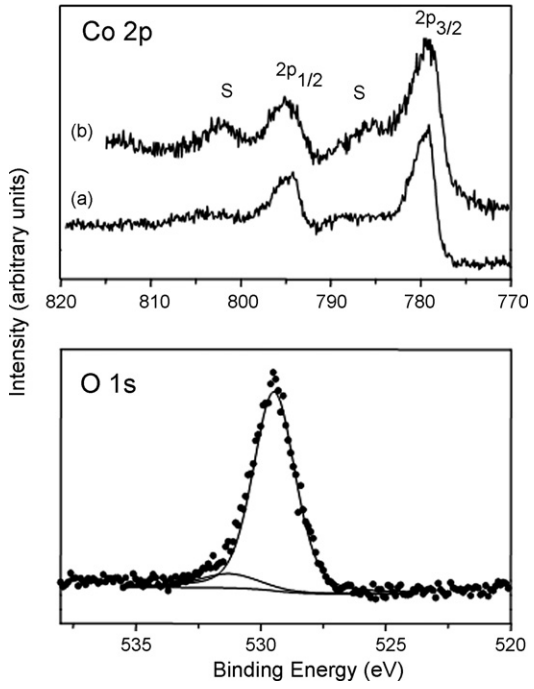

Fig. 11. XPS spectra for the UHV-conditioned (sputter/anneal) Co_3O_4(1 1 0) for Co 2p in (a) stoichiometric and (b) reduced, Cu-contaminated form, and for O 1s of the reduced form. Data were acquired with Mg Kα radiation.

3.3. Co_3O_4(1 1 1) surface

The other well formed, naturally occurring surface orientation for single crystals of the cobalt oxide spinel is Co_3O_4(1 1 1), which after surface conditioning shows the anticipated (1 1 1) hexagonal structure in LEED (Fig. 12) and Co 2p XPS comparable to the Co_3O_4(1 1 0) and CoO(1 0 0)/Co_3O_4 epitaxy. The O 1s peak shape, again, tails to higher binding energy (Fig. 13a) making it difficult to distinguish very low levels of surface hydroxylation due to problems in resolving the higher binding energy peak with an empirical fit to the data.

Contributions to the O 1s XPS peak from water and hydroxyl adsorption can be significant if the adsorbates are present in sufficient quantities. Fig. 13b shows the effects of exposure of the Co_3O_4(1 1 1) surface to 150 L H_2O (5 min at 6.6×10^{-5} Pa) at 110 K, which generates several monolayers of molecularly adsorbed water. At these low temperature conditions, there is insufficient energy to dissociate the water to form hydroxyls at the Co_3O_4(1 1 1) surface, however, and the water merely desorbs upon heating to 250 K (Fig. 13c).

Surface hydroxylation can be effected, however, by heating the Co_3O_4(1 1 1) substrate at 623 K under 6.6×10^{-5} Pa H_2O for 5 min. Cooling the substrate to 110 K under a 6.6×10^{-5} Pa H_2O background leads to both molecular and dissociative adsorption, as shown in Fig. 14. To remove the molecular water, the substrate is flashed briefly to 400 K, leaving only a surface layer of hydroxyl species.

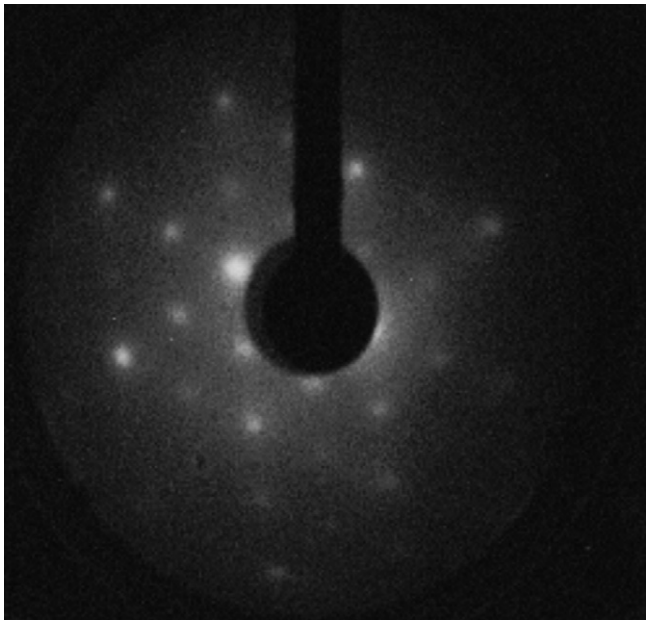

Fig. 12. LEED data for Co_3O_4(1 1 1) at an incident electron beam energy of 150 eV acquired at 300 K.

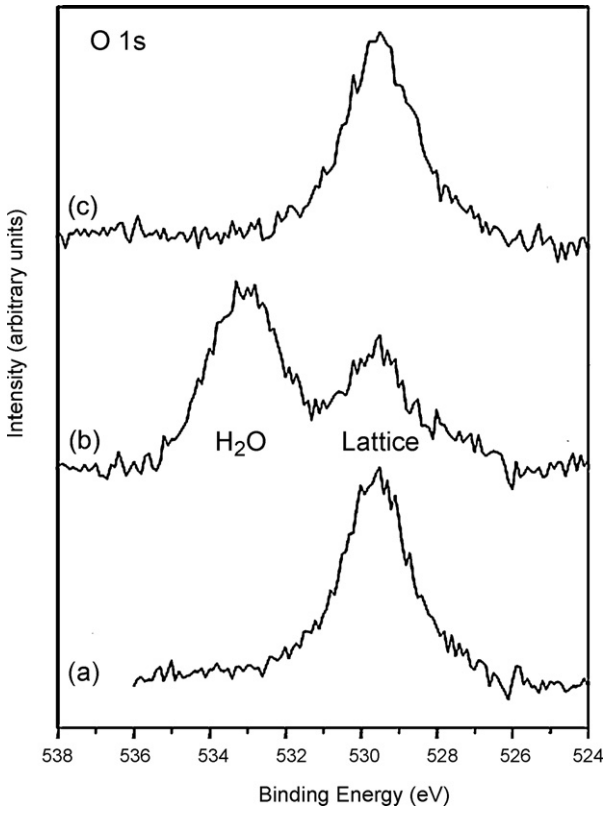

Fig. 13. O 1s XPS for Co_3O_4(1 1 1) for (a) the clean substrate, (b) after exposure to 150 L H_2O (5 min, 6.6×10^{-5} Pa) at 110 K resulting in molecular adsorption, and (c) after subsequent heating to 250 K to desorb the H_2O. Data were acquired with Mg Kα radiation.

The identity of the adsorbates is confirmed with HREELS analysis (Fig. 15), although both HREELS spectra require deconvolution of the multiple scattering peaks to resolve key features of the adsorbate spectrum. The water vapor cooled sample yields a very low intensity OH stretch in the 3600–3700 cm^{-1} (446.3–458.7 meV) region indicating that the OH stretching mode has a significant component of its motion parallel to the substrate plane. However, the H_2O libration and bending modes are clear indication of the molecular character of the adsorbate.

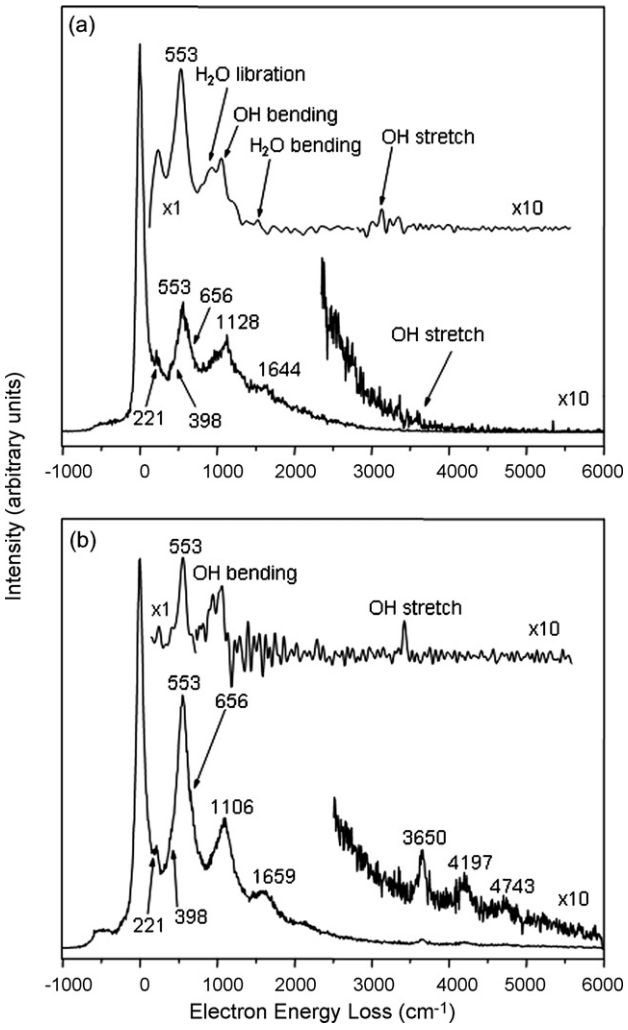

Fig. 15. HREELS spectra of Co_3O_4(1 1 1) surface (a) annealed under H_2O and (b) subsequently flashed to 400 K. Insets show deconvolution of the multiple scattering features. Spectra were acquired with a primary energy beam of 3.77 eV.

Upon flashing to 400 K, the molecular component of the water is desorbed, leaving the hydroxyl as the sole surface adsorbate. The hydroxyl species, which lies with its bond perpendicular to the surface, now shows an intense

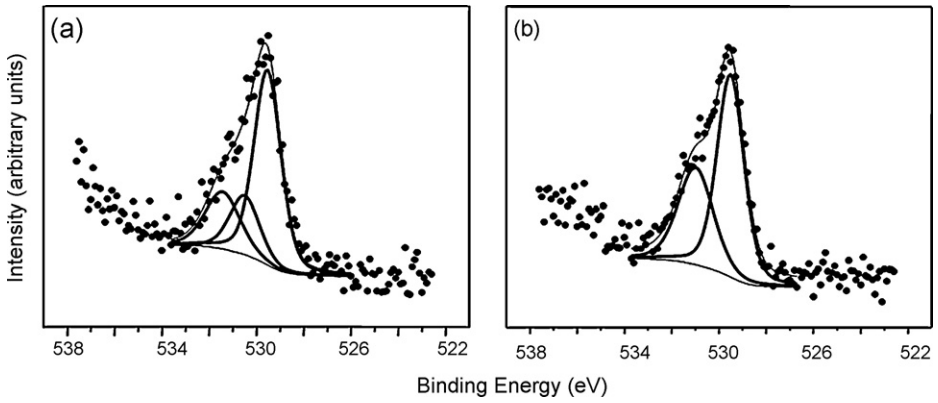

Fig. 14. O 1s XPS spectra Co_3O_4(1 1 1) surface (a) annealed under H_2O and (b) after flashing to 400 K. Data were acquired with Mg Kα radiation and were fitted with 40%/60% Lorentzian/Gaussian peaks after removal of a Shirley background.

OH stretch at 3650 cm^{-1} (452.5 meV) and a weaker bending mode at ~1100 cm^{-1} (136.4 meV) that overlaps with an intense multiple scattering feature in the original spectrum but is clearly present in the deconvoluted spectrum. Also found in the HREELS spectrum are the fundamental phonon modes at 211, 398, 553 and 656 cm^{-1} (26.2, 49.3, 68.6, and 81.3 meV, respectively), within error of the values reported for the Co_3O_4(1 1 0) substrate above. The relatively intense loss peaks at 4197 and 4743 cm^{-1} (520.4 and 588.1 meV) are multiple scattering features due to loss from the 558 cm^{-1} (69.2 meV) phonons plus 3650 cm^{-1} (452.5 meV) hydroxyl stretch and the combination phonon and OH bend at 1106 cm^{-1} (137.1 meV) plus 3650 cm^{-1} (452.5 meV) hydroxyl stretch, and are not found in the single-loss deconvoluted HREELS spectrum.

4. Discussion

Cobalt oxides show catalytic activity in partial oxidation and other heterogeneous surface reactions that depend upon the redox properties of the metal and the ability of the substrate to shuttle oxygen in a controlled manner. The close thermodynamic stability of the Co^{2+} and Co^{3+} oxidation states is a key feature in these mechanisms. Co^{2+} and Co^{3+} interconvert at CoO and Co_3O_4 single crystal surfaces quite readily, and the chemical environment of the cobalt cation in near surface layer of either oxide material can be adjusted between the two stoichiometric extremes under conditions easily achieved in UHV.

CoO(1 0 0) is the most stable orientation for CoO and bulk crystals of the monoxide cleave to present well ordered, stoichiometric surfaces due to the charge balanced and close packed nature of these non-polar planes. Heating under 10^{-4} to 10^{-2} Pa O_2 at 773 K slowly oxidizes the substrate to Co_3O_4 stoichiometry and, since the rocksalt and spinel oxygen sublattices are both fcc and equivalent in lattice spacing to within 5%, the oxidized thin films form in epitaxial arrangement. However, the (1 0 0) is not a preferred orientation for the spinel Co_3O_4, and the epitaxial growth ceases, or proceeds at an undetectably slow rate, after only about five monolayers.

During the oxidation process, cobalt photoemission shows distinct changes that are characteristic of spinel formation. The intense satellite structure of the Co 2p monoxide spectrum depends upon hybridization between high-spin Co^{2+} $3d^7$ and lattice anion O 2p states [21–23]:

$$\Psi_{\text{valence}} = \alpha 3d^n + \beta 3d^{n+1}\underline{L} + \gamma 3d^{n+2}\underline{L}^2 \quad (1)$$

Here, α, β, and γ are mixing parameters and $\underline{L}$ represents a hole in the oxygen 2p band resulting from a shift in electron density from O 2p to Co 3d upon hybridization. Upon photoemission, two possible final states are observed:

$$2p^6\Psi_{\text{valence}} + h\nu \rightarrow 2p^5 3d^8 + e^- \quad (2a)$$

$$\rightarrow 2p^5 3d^9\underline{L} + e^- \quad (2b)$$

and produce the satellite and main peaks, respectively. Upon Co_3O_4 formation, neither the full subshell of the low spin octahedral Co^{3+} nor the tetrahedrally coordinated Co^{2+} overlaps sufficiently with the O 2p levels to support the final state mechanism of Eq. (2b), and only very weak satellite features are observed in the Co 2p photoemission. Similar effects have been observed in the valence band region upon oxidation of CoO(1 0 0) to produce the CoO(1 0 0)/Co_3O_4 epitaxy using ultraviolet photoelectron spectroscopy (UPS) [7].

While the cobalt photoemission clearly indicates oxidation of the octahedral Co^{2+} cation to a Co^{3+} electronic environment, the phonon structure observed in HREELS is not sufficiently developed in the thin film layer to show all four fundamental phonons of the spinel lattice. This is unsurprising, since the phonon excitation is long range, extending 100 Å or more in the lattice, and the thin film should not be expected to have the same dielectric response as the surface region of the bulk spinel crystal. However, another significant difference in surface environment of the thin film epitaxy and Co_3O_4 bulk samples is the higher binding energy of the O 1s XPS feature associated with the epitaxy.

Both CoO and Co_3O_4 materials show O 1s lattice binding energies of 529.4 eV for clean, stoichiometric surfaces. O 1s binding energies in the range of 531.2 eV, found for the epitaxy, are generally attributed to oxide defect states, differential charging, or surface hydroxylation. Hydroxylation, in any sufficient quantity, can be ruled out for the CoO(1 0 0)/Co_3O_4 epitaxy since the HREELS spectrum does not show any electron loss features resulting from the OH adsorbate vibrational spectrum. Such losses are clearly visible for Co_3O_4(1 1 0)-OH and Co_3O_4(1 1 1)-OH HREELS adsorbate spectra. The shift in binding energy cannot be assigned to differential charging since no corresponding shifts are observed in the Co 2p XPS spectra.

The higher O 1s binding energy for the CoO(1 0 0)/Co_3O_4 epitaxy must thus be due to a different environment for the oxygen lattice ions in the epitaxy. Similar peaks have been assigned to defect species for adsorbed oxygen, improperly incorporated into the oxide lattice, although it is unlikely that oxygen related to an adsorbate state could result in a multilayer epitaxial feature. However, it is possible that the filling of tetrahedral and octahedral sites by the cobalt cations is not as well ordered or otherwise differs from that found in bulk Co_3O_4. In surface analysis, higher binding energy O 1s XPS features are generally assigned to surface hydroxylation without corroborating information from HREELS, FTIR, or other techniques. While this might be a reasonable expectation for air-exposed oxides, the present studies illustrate that the assignment is not unique, and should be made with caution.

5. Conclusion

CoO(1 0 0), Co_3O_4(1 1 0) and Co_3O_4(1 1 1) single crystal substrates have been investigated with X-ray photoelectron spectroscopy (XPS), high-resolution electron energy loss spectroscopy (HREELS) and low energy electron diffraction (LEED) for their surface reactivity toward O_2 and H_2O and for their stability under reducing UHV conditions. There is facile interconversion between CoO and Co_3O_4 stoichiometry at the oxide surface, which despite the compositional variability, remains

well ordered in long-range structure. Oxidation of the monoxide results in a CoO(1 0 0)/Co_3O_4 epitaxy which does not form in the stable Co_3O_4(1 1 0) and Co_3O_4(1 1 1) orientations due to templating effects of the underlying CoO(1 0 0) substrate. This leads to a thin film structure with somewhat different characteristics than the surface found on the naturally occurring orientations of the bulk spinel, including a shift in O 1s binding energy and a more poorly developed Fuchs–Kliewer phonon spectrum. Contrary to reports of a pressure gap that creates difficulty in oxide hydroxylation under UHV, it is possible to hydroxylate oxide substrates with H_2O, provided sufficient activation is available to dissociate the water molecule.

Acknowledgement

We gratefully acknowledge support from the National Science Foundation through NSF grant CHE-0213320.

References

[1] A. Zecchina, D. Scarano, S. Bordiga, G. Spoto, C. Lamberti, Adv. Catal. 46 (2001) 265–397.
[2] N. Barsan, D. Koziej, U. Weimar, Sens. Actuators B121 (2007) 18–35.
[3] S. Greenwald, Acta Crystallogr. 6 (1953) 396–398.
[4] W. Jauch, M. Reehuis, H.J. Bleif, F. Kubanek, P. Pattison, Phys. Rev. B 64 (2001) 0521002/1–0521002/3.
[5] W.L. Smith, A.D. Hobson, Acta Crystallogr. B29 (1973) 362–363.
[6] W.L. Roth, J. Phys. Chem. Solids 25 (1964) 1–10.
[7] M.A. Langell, M.D. Anderson, G.A. Carson, L. Peng, S. Smith, Phys. Rev. B 59 (7) (1999) 4791–4798.
[8] S.C. Petitto, M.A. Langell, Surf. Sci. 599 (2005) 27–40.
[9] Kindly provided by W.H. McCarroll, Department of Chemistry, Biochemistry and Physics, Rider University, Lawrenceville, New Jersey, USA.
[10] R.W.M. Kwok, available from: http://www.phys.cuhk.edu.hk/~surface/XPSPEAK.
[11] D. Shirley, Phys. Rev. B 5 (1972) 4709–4714.
[12] J. Vegh, J. Electron Spectrosc. Rel. Phenom. 151 (2006) 159–164.
[13] P.A. Cox, W.R. Flavell, A.A. Williams, R.G. Egdell, Surf. Sci. 152/153 (1985) 784–790.
[14] E.M. Malone, S.C. Petitto, G.S. Harbison, K.W. Wulser, M.A. Langell, J. Vac. Sci. Technol. 23 (2005) 1061–1066.
[15] T.J. Chuang, C.R. Brundle, D.W. Rice, Surf. Sci. 59 (1976) 413–429.
[16] M.M. Natile, A. Glisenti, Chem. Mater. 17 (2005) 3403–3414.
[17] H.A. Hagelin-Weaver, G.B. Hoflund, D.M. Minahan, G.N. Salaita, Appl. Surf. Sci. 235 (2004) 420–448.
[18] D. Briggs, J.T. Grant, Surface Analysis by Auger and X-ray Photoelectron Spectroscopy, IM Publications, Chickester, UK, 2003.
[19] Thermodynamic data available on NIST webbook from: http://webbook.nist.gov/chemistry/.
[20] M. Wuttig, X. Liu, Ultrathin Metal Films, Springer Tracts in Modern Physics, vol. 206, Springer-Verlag Publishers, Berlin, 2004.
[21] U.D. Wdowik, K. Parlinski, Phys. Rev. B 75 (2007) 104306/1–104306/6.
[22] S. Sindhu, M. Heiler, K.M. Schindler, W. Widdra, H. Neddermeyer, Surf. Sci. 566/567 (2004) 471–475.
[23] Z.X. Shen, J.W. Allen, P.A.P. Lindberg, D.S. Dessau, B.O. Wells, A. Borg, W. Ellis, J.S. Kang, S.J. Oh, I. Lindau, W.E. Spicer, Phys. Rev. B 42 (1990) 1817–1828.
[24] E.M. Malone, S.C. Petitto, M.A. Langell, Solid State Commun. 130 (9) (2004) 571–575.
[25] G.A. Carson, M.H. Nassir, M.A. Langell, Surf. Sci. Spectra 5 (1998) 235–244.
[26] G. Heiland, H. Ibach, H. Lueth, W. Moench, Surf. Sci. 35 (1973) 425–426.
[27] Y.L. Li, K.L. Yao, Z.L. Liu, Surf. Sci. 601 (2007) 876–882.
[28] Y. Oda, S. Mizuno, S. Todo, E. Torikai, K. Hayakawa, Jpn. J. Appl. Phys. 37 (1998) 4518–4521.
[29] H. Shirai, Y. Morioka, I. Nakagawa, J. Phys. Soc. Jpn. 5 (1982) 592–597.
[30] M. Lenglet, B. Lefez, Solid State Commun. 98 (1996) 689–694.
[31] S.C. Petitto, M.A. Langell, J. Vac. Soc. Technol. A 22 (2004) 1690–1696.